

## Article

# Friction and Wear Characteristics of Cr-CNTs Composite Coating End Faces of High-Temperature Mechanical Seals

Haichao Yang, Shuangxi Li \*, Runmei Ma, Guoqing Zhang and An Liu

College of Mechanical and Electrical Engineering, Beijing University of Chemical Technology, Beijing 100029, China; yanghaichao20@163.com (H.Y.); marm@mail.buct.edu.cn (R.M.); 18813186787@163.com (G.Z.); 15261730248@163.com (A.L.)

\* Correspondence: 2003500008@buct.edu.cn

**Abstract:** To improve the reliability of the end faces of high-temperature mechanical seals, a high-performance composite material that introduces carbon nanotubes (CNTs) into the laser-melted Cr coating is proposed. In this study, for high-temperature and high-speed mechanical seals under actual working conditions, friction and wear tests were conducted under different working conditions and using different end face materials. The high-temperature tribological properties of the Cr-CNTs coatings were analyzed, and the strengthening mechanism of the Cr-CNTs coatings on end faces was investigated. The results indicate that the wear resistance of the Cr-CNTs coating at high temperatures is first enhanced and then weakened with the increase in the CNTs content. The composite coating end face performance is optimal when the CNTs content is 10 wt%. The presence of CNTs between the end faces when grinding against the graphite ring favors the generation of a graphite film. The coefficient of friction of the Cr-CNTs coating is reduced by at least 12.46% compared to the Cr coating at a temperature of 483 K. This study provides reference examples for the application of carbon nanotubes in high-performance mechanical seals and new research ideas for improving the performance of mechanical seal end faces.

**Keywords:** carbon nanotubes; composite coating; friction and wear; mechanical seal; end face strengthening; wear mechanism



**Citation:** Yang, H.; Li, S.; Ma, R.; Zhang, G.; Liu, A. Friction and Wear Characteristics of Cr-CNTs Composite Coating End Faces of High-Temperature Mechanical Seals. *Coatings* **2023**, *13*, 1692. <https://doi.org/10.3390/coatings13101692>

Academic Editor: Jurgita Zekonyte

Received: 17 August 2023

Revised: 25 September 2023

Accepted: 25 September 2023

Published: 27 September 2023



**Copyright:** © 2023 by the authors. Licensee MDPI, Basel, Switzerland. This article is an open access article distributed under the terms and conditions of the Creative Commons Attribution (CC BY) license (<https://creativecommons.org/licenses/by/4.0/>).

## 1. Introduction

With the increasing demand for improved contact mechanical seal end face performance, mechanical seal end face surface modification technology has been widely used, and composite coatings in high-parameter condition mechanical seals have made significant progress in research [1–4]. The composite coating is essential to improve the seal end face's stability and wear resistance and to extend the mechanical seal's life [5–8]. Research on the impact of composite coatings on seal end face wear and the strengthening mechanism of composite coating materials is currently one of the hot spots of scholars' research.

Cr and its alloy coatings have the advantages of high heat resistance, high wear resistance, and high finish, and have good adhesion and chemical stability when combined with the substrate. Cr alloy coatings are used in various industrial applications [9–11], such as high-temperature fuel casing protection, aerospace corrosion protection, valve wear protection, etc. Jiahong et al. [12] compared the effect of Cr and Ni content on the friction and wear behavior of laser cladding coated Cr-Ni alloy coatings at high temperatures and found that the increase in the Cr content is the main factor in improving the high-temperature wear resistance of CrNi alloy coatings. The results of thermal fatigue cycling studies of coatings by Wang et al. [13] indicated that as the chromium content of the chromium alloy coatings increased, the total crack length of the alloy decreased, and the thermal fatigue properties of the alloys increased significantly. Friction and wear tests by Günen et al. [14] and Guo et al. [15] have demonstrated that the addition of appropriate amounts of Cr has a

strengthening effect on the properties of coatings, which is mainly reflected in the improvement of microhardness, wear resistance at high temperatures, and oxidation resistance. Drozd et al. [16] further improved the oxidation resistance by depositing a small amount of yttrium additive on the Cr coating. However, the high preparation cost makes it difficult for their research results to be widely used in the field of mechanical seals. Litovka et al. [17] explored the reinforcing effect of nanodiamond (DLC) films and carbon nanotubes on Cr coatings and found that Cr coatings with added carbon nanomaterials (nanodiamonds and carbon nanotubes) have higher wear resistance and microhardness, are cheaper to produce, and are more competitive than similar products. However, the strengthening mechanism of Cr coatings by CNTs needs to be further investigated.

With the continuous development of composite coating technology, carbon nanotubes (CNTs) have come to the attention of tribologists. Due to their unique spatial structure and physical properties, CNTs have the same high hardness as diamond and have good toughness and tensile strength, making them a new reinforced and toughened material that needs to be studied urgently [18–20]. EL-Kashif et al. [21] concluded that CNTs are beneficial to avoid friction cracks and fins on the surface of friction materials, and their application in automotive brake friction materials helps reduce temperature rise, noise, and vibration. Reinert et al. [22] and Lai et al. [23] deeply analyzed the mechanism of CNTs to improve the tribological performance of composite coatings and found that CNTs shed from the coating surface due to wear can effectively enhance the self-lubrication of the end face and reduce the end face wear. Hai-dou Wang et al. [24] found that the non-shedding CNTs on the coating surface tended to roll perpendicular to the friction direction, which could enhance the effect of self-lubrication of the coating. G. J. Wang et al. [25] comparatively investigated the mechanical properties of copper and CNTs composite copper coatings and found that the addition of CNTs increased the strength and elastic modulus of the coatings. Roy et al. [26] investigated the thermomechanical properties of polyimide/multi-walled CNTs steel-based composite coatings at a high temperature of 473 K. Incorporating multi-walled CNTs reduced the composite coatings' thermal degradation and enhanced the composites' wear resistance and mechanical properties. The reinforcing effect of CNTs on coatings and the reinforcement mechanism have been verified in a variety of reciprocating friction tests. However, few scholars have designed rotary friction tests for mechanical seal structures.

Cr and its composite coating can effectively improve the stability and wear resistance of the end face of the substrate under high-temperature working conditions, and the addition of CNTs to the coating material can increase the hardness and improve the tribological properties of the material. In this paper, Cr-CNTs coatings were selected for the study of high temperature friction and wear behavior in combination with the working principle of mechanical seals rotating against grinding. The effects of different CNTs contents and different temperatures on the overall tribological properties of the coatings were systematically investigated, and the low-cost and efficiently prepared Cr-CNTs coating materials for high-temperature mechanical seals were initially obtained. Aiming at the actual state of mechanical seal application, the strengthening mechanism of Cr-CNTs coating on the comprehensive performance of the end face under high-temperature working conditions was initially discussed.

## 2. Materials and Methods

The purified CNTs powders (\*multi-walled carbon nanotubes, 8–15 nm OD, 3–12  $\mu\text{m}$  length) were mixed, respectively, with high purity Cr powder (30–38  $\mu\text{m}$  particle size) at 0 wt%, 5 wt%, 10 wt%, 15 wt%, and 20% mass fraction. The 5 mm diameter agate balls were mixed with the powders in a 1:3 volume fraction, and the CNTs and Cr powders were homogeneously dispersed by a planetary ball milling machine (\*speed 300  $\text{r}\cdot\text{min}^{-1}$ , running time 6 h, change of direction of rotation every hour) [27].

Cr-CNTs coatings were prepared on the end faces of S30406 metal rings by laser cladding (RFL-C6000, power 1400 W, scanning speed 250  $\text{mm}\cdot\text{min}^{-1}$ , powder feeding rate

30 g·min<sup>-1</sup>, air flow 4 L·min<sup>-1</sup>) [28], and the end faces were ground and polished. The elemental content of the substrate material is shown in Table 1. The end face roughnesses were all Ra = 0.008 μm, and the coating thicknesses were all 0.5 mm. SEM scanning electron microscopy was used to observe the microscopic powders before laser cladding and the morphology of the coating end face after laser cladding, as shown in Figure 1. The coverage area of CNTs on Cr particles was enhanced with the increase in content (Figure 1a–c). The thickness of CNTs on the surface of Cr particles gradually becomes thicker and unevenly distributed as the content of CNTs continues to increase (Figure 1c). The color of the final Cr coating surface gradually deepened (Figure 1d–h).

**Table 1.** Substrate material (wt%).

Substrate Material	Cr	Ni	Mn	Si	N	P	C	Fe
S30406	19.93	10.08	1.16	0.26	0.06	0.04	0.04	Bal.

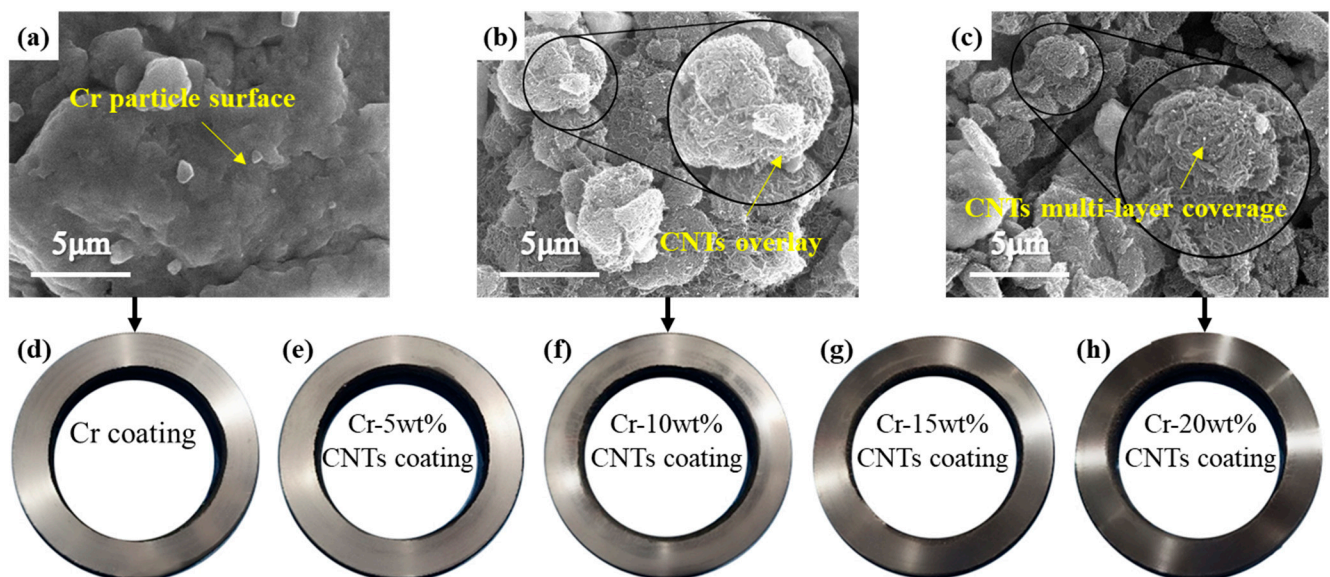


**Figure 1.** Composite powders and composite coatings with different CNTs contents: (a–c) composite powders microscopic morphology, (d–h) composite coating macroscopic morphologies.

SEM scanning electron microscope observation test pieces were prepared by WEDM to observe the coating end face and cross-section morphology after laser cladding. Due to the unavoidable reaction of the Cr coating with the atmospheric C and O elements during the laser cladding and grinding process, a small amount of granular alloy impurities will exist on the surface, which can affect the continuity of the end face crystals of the coating (Figure 2a,d). When the CNT content was 10 wt%, the C element was uniformly distributed, and the alloy coating grains formed were uniform and dense. CNTs decompose into C atoms under the high temperature of the laser beam, react with Cr elements, and reform high hard alloys that are difficult to react with other elements and are uniformly distributed in the coating (Figure 2b,e). CNTs have the effect of refining grains to enhance the continuity of the material [29]. Whether intact CNTs were still present in the coatings needed to be analyzed in conjunction with the Raman spectroscopy test results (Figure 3). Based on the analysis of the Raman spectrogram of the cross-section, the curve of the Cr coating was smooth with fewer C elements. When the content of CNTs was 10 wt% and 20 wt%, there were obvious D and G peaks in the cross-section. Because the ratio of the heights of the two peaks in the curves before and after laser melting is similar, it can be judged that intact CNTs exist in both coatings [30]. When the CNTs content reached 20 wt%, although the particle size in the coating formed after laser melting was further reduced,

pores appeared on the surface, and C elements aggregated at the pores (Figure 2c,f). This is because the surface of the Cr particles before laser melting coating was wrapped with thicker CNTs, and the thickness of the wrapping was not uniform (Figure 1c). Excess C in the laser cladding process tends to react with O to form CO<sub>2</sub>, which cannot escape before forming pores, eventually forming defects in the coating.

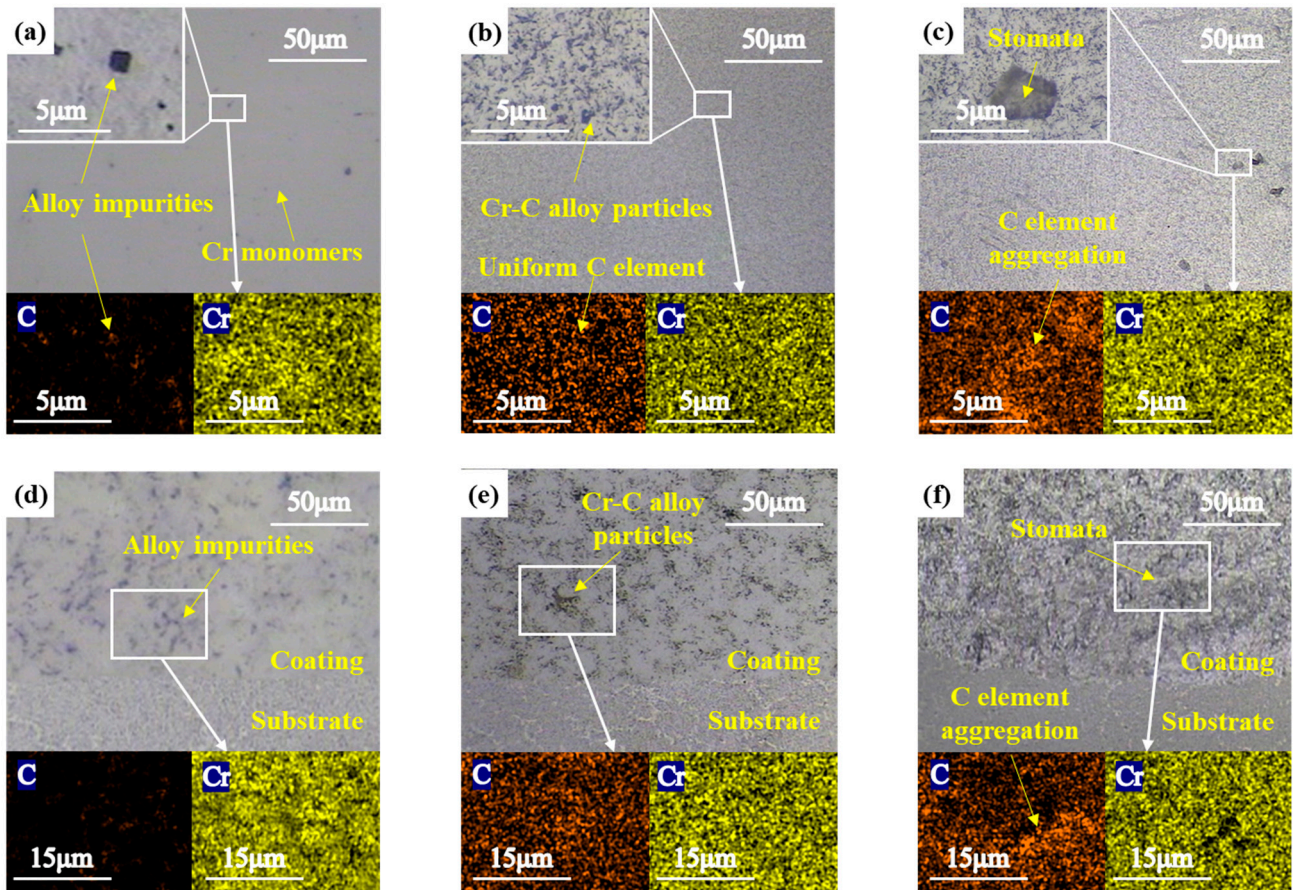


**Figure 2.** The coating end face and cross-section morphology after laser cladding: (a–c) end face morphology and elemental mappings images, (d–f) cross-section morphologies and elemental mappings images.

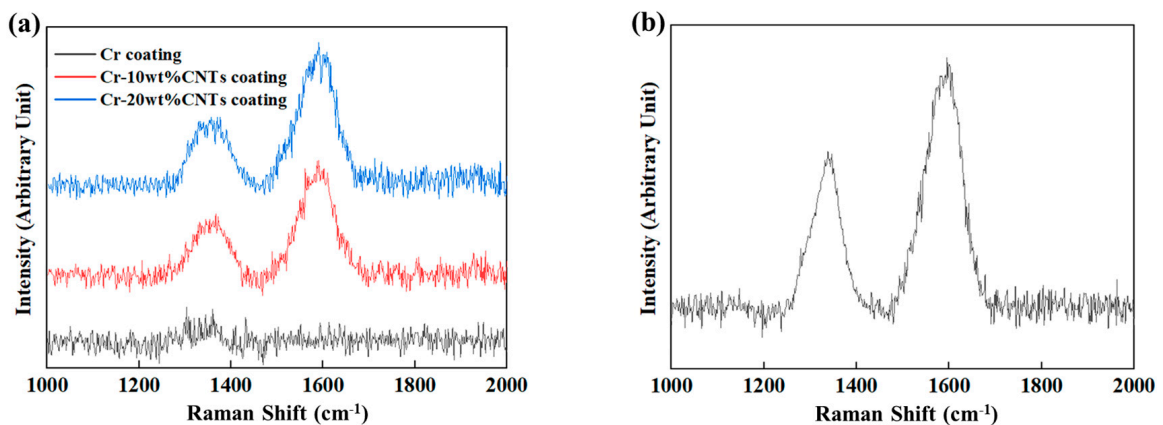


**Figure 3.** Raman spectroscopy test results: (a) coating after laser cladding, (b) CNTs powder before laser cladding.

The friction and wear tests of different coated dynamic and static ring pairs were carried out using the PlintTE-92 friction and wear tester, the structure of which is shown in Figure 4. Friction and wear tests were performed on test pieces with different CNTs contents as shown in Table 2. In the project that this paper depends on, the equipment needs a Cr-coated dynamic ring and an MF-307 graphite static ring to realize the mechanical seal under oil lubrication,  $6000 \text{ r}\cdot\text{min}^{-1}$ , and end face specific pressure of 0.6 MPa. The upstream of the equipment can generate heat, but it is difficult to dissipate the heat in time, and the maximum temperature in the mechanical seal chamber reaches 483 K. In this paper, several temperature gradients are set to meet the friction and wear phenomenon of actual working conditions, and the friction and wear performance of coatings at high temperatures is explored. Due to the initial startup of the mechanical seal, the lubricant fails to enter the seal end face, and the dry friction phenomenon is likely to occur. Therefore, it is necessary to study the friction and wear state of the test piece under dry friction conditions. Setting the working conditions as a dry friction SiC ball wear test, the effect of carbon nanotube content on the wear resistance of the end face can be more intuitively investigated.

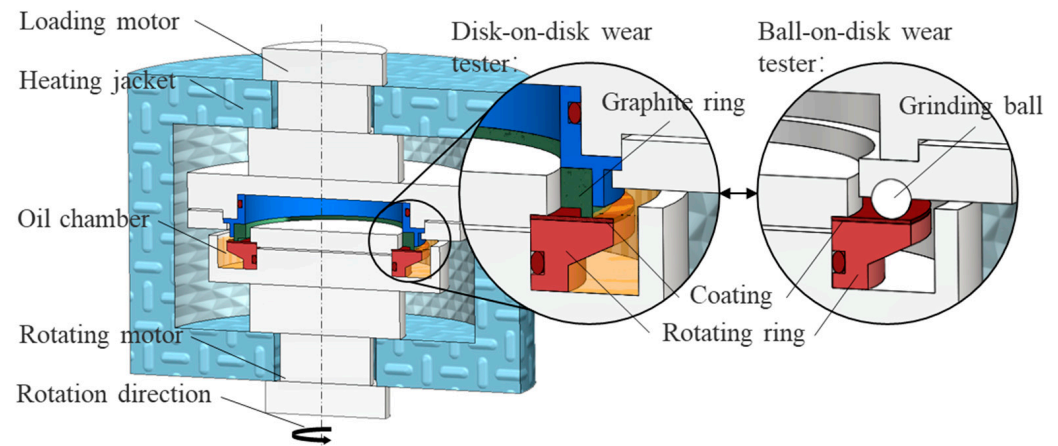


Figure 4. Friction and wear test structure.

Table 2. Wear test parameters.

Test Method	Lubrication Condition	Temperature/K	Load/N	Speed/ $\text{r}\cdot\text{min}^{-1}$	Time/s
Ball-on-disk test with SiC grinding ball	Dry friction	293	75	6000	600
		348			
		393			
		438			
		483			
Disk-on-disk test with MF-307 graphite ring	Dry friction	293	75	6000	600
		348			
		393			
		438			
		483			
	Oil lubrication	293	75	6000	600
		348			
		393			
		438			
		483			

### 3. Results

#### 3.1. Effect of CNTs Content

The ball-on-disk test with end face specific pressure of 0.60 MPa and rotational speed of 6000 r·min<sup>-1</sup> was carried out, and the heating temperatures were set, respectively, to 293 K, 348 K, 393 K, 438 K, and 483 K to analyze the effect of CNTs content on the wear resistance of the coatings. The friction coefficients of the five Cr-CNTs coatings at different heating temperatures are shown in Figure 5a–e, and the variation rule of the average friction coefficient of the Cr-CNTs coatings with heating temperatures is shown in Figure 5f.

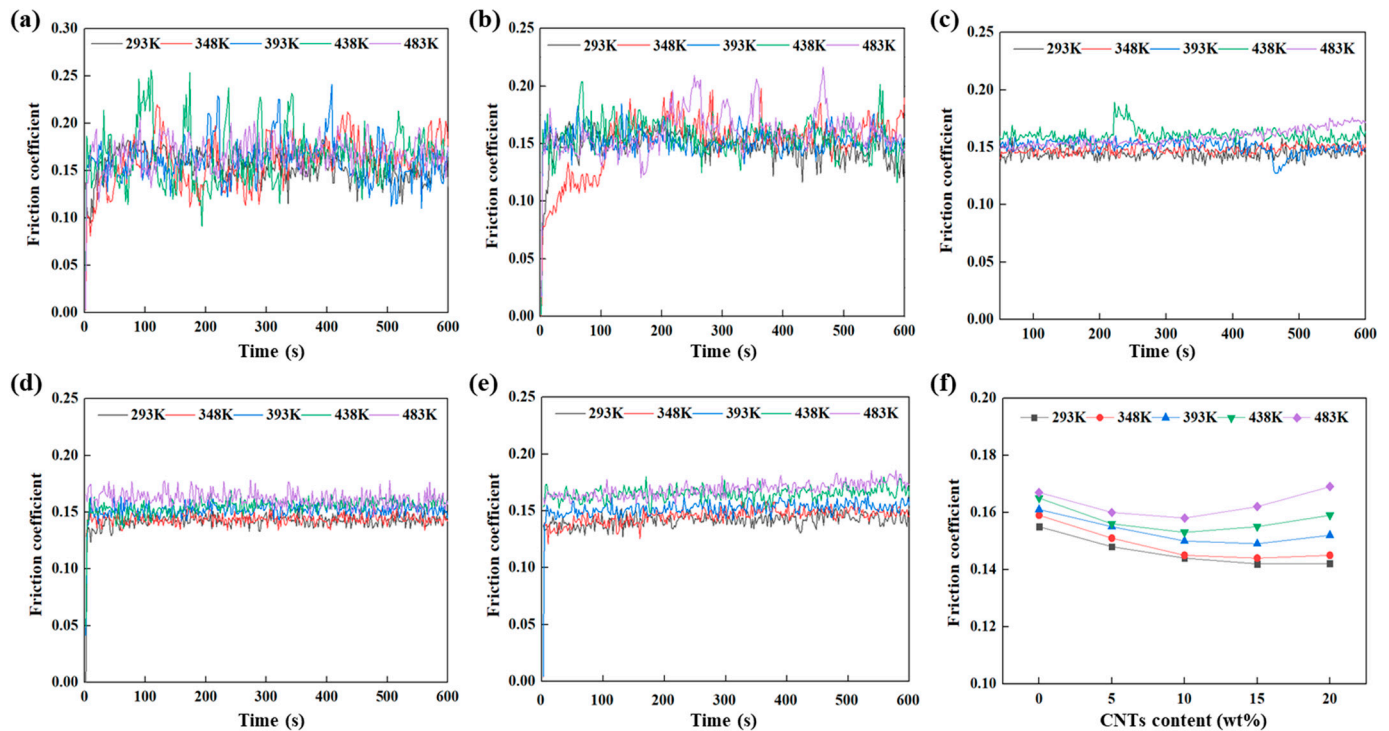


**Figure 5.** Influence of CNTs content on friction coefficient at different media temperatures: (a) Cr coating, (b) Cr-5 wt% coating, (c) Cr-10 wt% coating, (d) Cr-15 wt% coating, (e) Cr-20 wt% coating, (f) the average friction coefficient.

The coefficient of friction increases with increasing heating temperature for the same CNTs content because the heating temperature directly affects the end face temperature. When the end face temperature increases, the expansion and deformation of the end face micro-convex body is enhanced, the degree of wear increases, and the coefficient of friction increases [31]. A comparison of Figure 5a–e shows that the addition of CNTs effectively reduces the range of fluctuation of the friction coefficient of the Cr coating. When the content of CNTs is lower than 10 wt%, the fluctuation of the friction coefficient decreases with the increase in CNTs content (Figure 5a–c). However, when the content of CNTs is more than 10 wt%, the effect of the CNTs on the reduction of the friction coefficient fluctuation is not apparent (Figure 5c–e). This is because the appropriate amount of CNTs improves the continuity of the coating end face, enhances the mechanical properties of the laser-fused coating, and strengthens the end face wear resistance [32]. A comparison of Figure 5a–e shows that the addition of CNTs effectively reduces the range of fluctuation of the friction coefficient of the Cr coating. However, too high a content of CNTs will lead to a decrease in the quality of the coating preparation and a weakening of the end face wear resistance at high temperatures.

As shown in Figure 5f, the coefficient of friction decreases with increasing CNTs content at 293 K and 348 K media temperatures, and the decrease happens gradually. At higher heating temperatures, the friction coefficient first decreases with increasing CNTs content, and the friction coefficient is lowest at 10 wt% CNTs content. Then, it increases with the increase in CNTs content, and the magnitude of the increase rises with the increasing heating temperature. Even at 483 K, the friction coefficient of the Cr-CNTs coating with 20 wt% CNTs content is higher than that of the Cr coating. Although excessive CNTs will lead to poorer end face quality and exacerbate the wear effect, the wear-reducing effect of CNTs on the coating surface can moderate the phenomenon when the heating temperature is low and the change in the friction coefficient with the content of CNTs is more stable. When the heating temperature is higher, the wear of the coatings with poorer coating quality is further aggravated, and the effect of the aggravated wear exceeds the wear-reducing effect of CNTs on the coating surface. Therefore, the coefficient of friction decreases and then increases with the content of CNTs at higher heating temperatures.

The test temperature was 483 K. The microscopic surface morphology and energy spectrum analysis of different test pieces are shown in Figure 4. There are many craters on the Cr coating caused by adhesive wear. The edges of the craters are in the form of refined grains (Figure 6a). Due to the high friction coefficient of the end face under dry friction SiC pairing conditions, the adhesive wear is worse, and the edges of the pits of the stripping layer are continuously subjected to abrasion and broken in granular form. Zooming in on a crater's edge, spherical particles with high O elements can be observed (Figure 6b). Some Cr and other tramp metals oxidize to create abrasive particles that add to the wear [33].

The Cr-5 wt% CNTs coating is also dominated by adhesive wear. The edges of the stripping layer craters are flatter. At the same time, a small number of linear abrasions caused by abrasive grain wear are present (Figure 6c). Zooming in on the edge of a crater, a small number of striped CNTs particles can be found in addition to a small number of abrasive particles (Figure 6d). The Cr-10 wt% CNTs coating showed less adhesive wear (Figure 6e). The number of CNTs particles increases, and the C specific gravity increases significantly. Many CNTs are extruded to sheet CNTs films that can reduce wear (Figure 6f).

The Cr-15 wt% CNTs coating has less adhesive wear and is dominated by abrasive wear with the presence of large pores (Figure 6g). A large number of CNTs are distributed around the stomata, with a decrease in the proportion of O elements and an increase in the proportion of C elements (Figure 6h). The distribution of the pores on the end face of the Cr-20 wt% coatings is denser (Figure 6i), the abrasive wear is aggravated, and the specific gravity of the C element at different locations varies greatly (Figure 6j). Excess CNTs increase the self-lubrication of the coating but also lead to an increase in end-face porosity and a deterioration in the quality of the coating overlay.

The three-dimensional morphology of the end face abrasion marks of Cr coatings with different contents of CNTs was observed by laser confocal microscopy, as shown in Figure 7. The Cr coating end face has deeper wear marks, and the cross-section is in the shape of a pit with a deep center and shallower sides. The Cr-5 wt% CNTs coating end face is in the shape of a pit with shallow wear marks, and the form of the wear is dominated by adhesive wear. The Cr-10 wt% CNTs coating end face wear marks have a more uniform depth distribution in the cross-section and a shallower average wear depth. As the content of CNTs increases, the CNTs shed during end face wear play a lubricating role. Adhesive tearing between end faces is reduced, and abrasive particle collisions between micro-convex bodies on the end faces are increased. The form of wear changes from predominantly adhesive wear to predominantly abrasive wear [34]. When the CNTs content exceeds 10 wt%, as the CNTs content continues to increase, the depth distribution of abrasion marks on the end face of the coating becomes more uniform, and the average depth gradually increases.

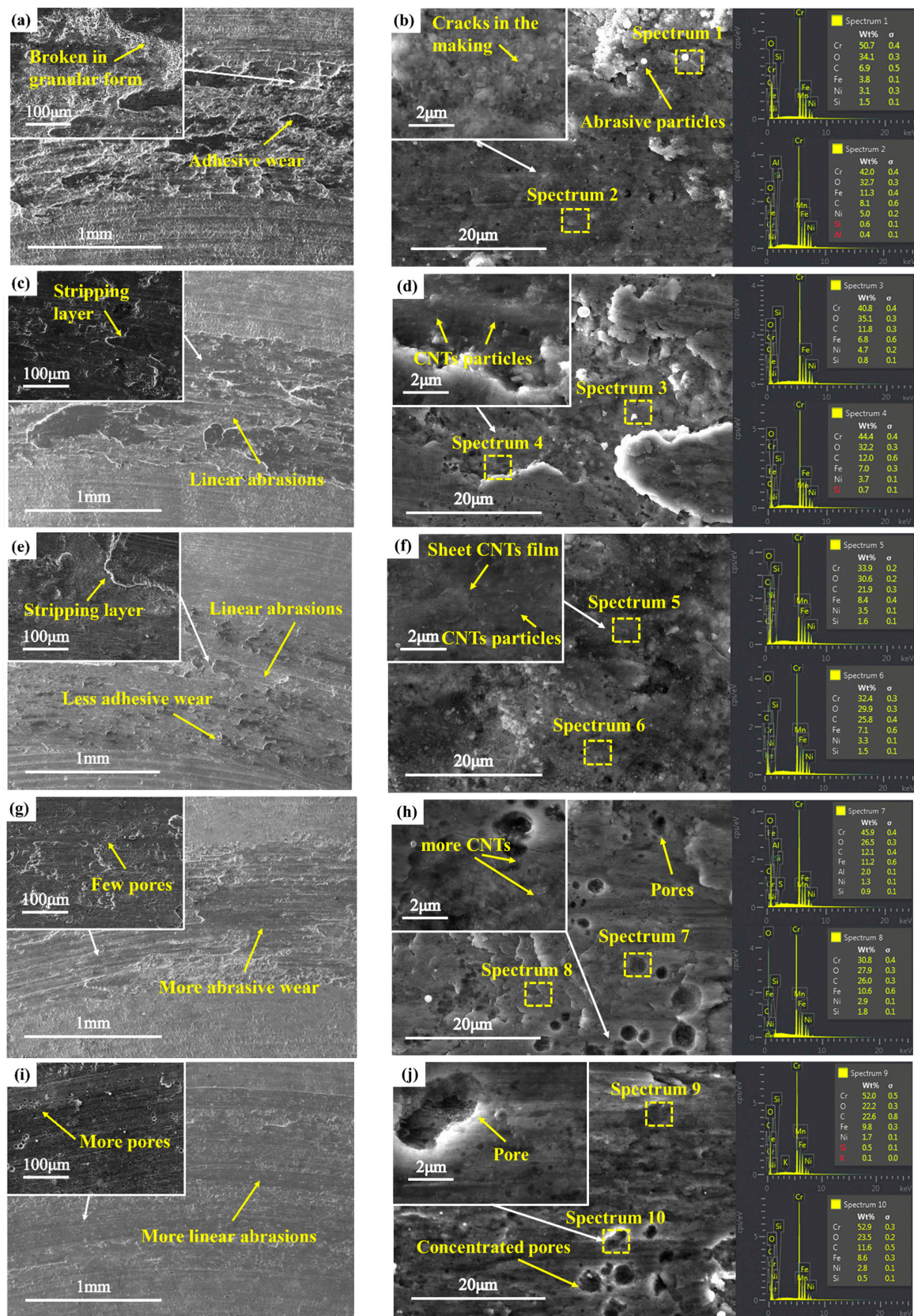


**Figure 6.** Scanning electron microscopy and energy spectrum analysis images of composite coatings: (a,b) Cr coating, (c,d) Cr-5 wt% CNTs coating, (e,f) Cr-10 wt% CNTs coating, (g,h) Cr-15 wt% CNTs coating, (i,j) Cr-20 wt% CNTs coating.

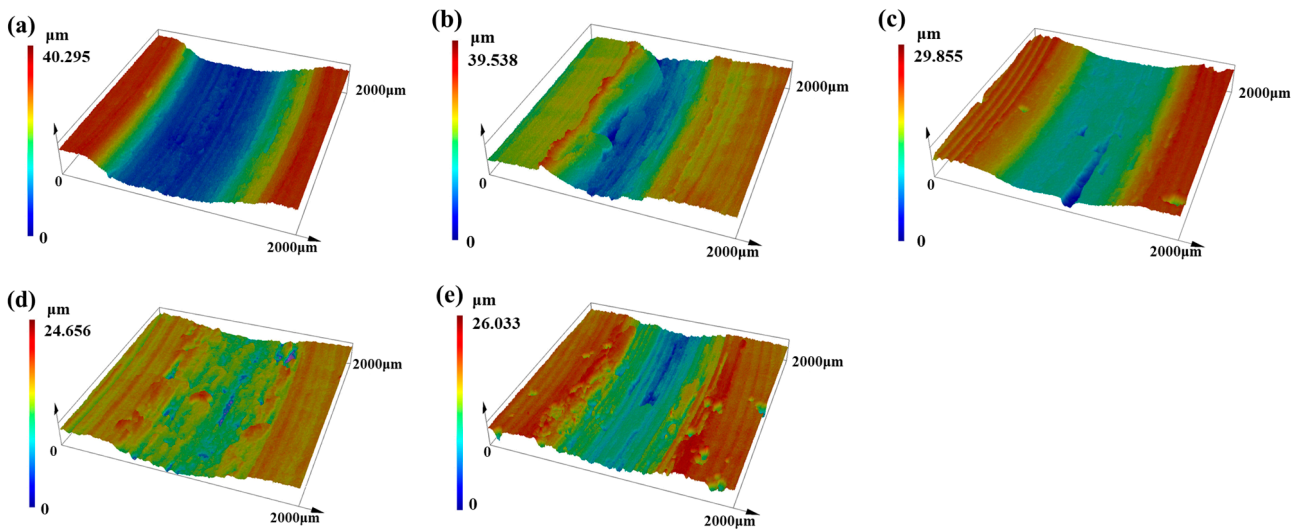


**Figure 7.** Laser confocal micrographs of composite coatings: (a) Cr coating, (b) Cr-5 wt% CNTs coating, (c) Cr-10 wt% CNTs coating, (d) Cr-15 wt% CNTs coating, (e) Cr-20 wt% CNTs coating.

Cross-section hardness measurements were used to measure the hardness of Cr coatings with different CNTs contents. The average wear depth and average cross-section hardness curves of coatings with different CNTs contents are shown in Figure 8. With the increase in CNTs content, the average wear depth of the Cr-CNTs coatings shows a trend of decreasing and then increasing, and the average wear depth is the smallest when the CNTs content reaches 10%. The hardness of the Cr-CNTs coatings increases linearly with increasing CNTs content when the CNTs content is lower than 10 wt%. When the CNTs content reaches 15 wt%, the hardness of the Cr-CNTs coatings starts to show a small decrease. When the CNTs content increases to 20 wt%, the hardness of the Cr-CNTs coating decreases significantly. The combination of the appropriate amount of CNTs and Cr coating increases the hardness [35], improving the wear resistance and self-lubricating property of the coating so that the average depth of wear is minimized when the content of CNTs is 10 wt%. Excess CNTs will result in inadequate fusion bonding within the coating so that the surface hardness is drastically reduced. The Cr-10 wt% CNTs coating has both excellent self-lubrication and wear resistance.

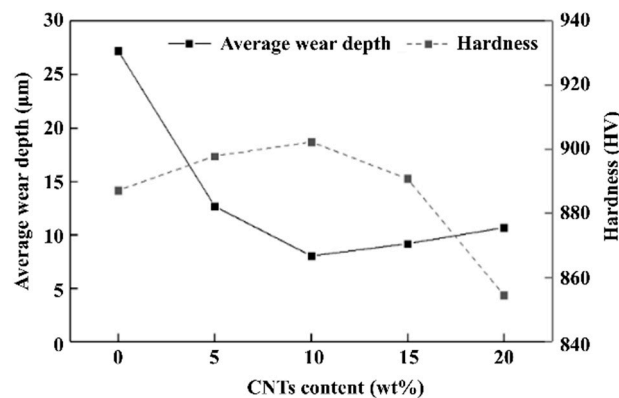


**Figure 8.** Average wear depth and hardness curves of composite coatings.

### 3.2. Effect of End Face Material

The test temperature was 438 K, and the rotational speed was  $6000 \text{ r}\cdot\text{min}^{-1}$ . The friction coefficients of the uncoated, Cr-coated, and Cr-10 wt% CNTs coatings with the MF-307 graphite ring end faces after grinding are shown in Figure 7. Under the dry friction condition (Figure 9a), the end face friction coefficient of the Cr-CNTs coating is the smallest

and the time required for stabilization is the shortest. Graphite powder shed on the end face of the graphite ring due to abrasion builds up on the friction end face and can form a graphite film with a wear-reducing effect. The CNTs between the end faces of the Cr-CNTs coating facilitate the buildup of graphite powder, generating a more uniform and stable graphite film for the same running time. Under the oil lubrication condition (Figure 9b), the Cr-CNTs coating has optimal wear reduction. The graphite shedding and stacking efficiency is reduced in the presence of oil film. However, the graphite film with high coverage can still be generated between the end surfaces of the Cr-CNTs coatings, which enables the graphite film and the oil film to play the role of wear reduction together.

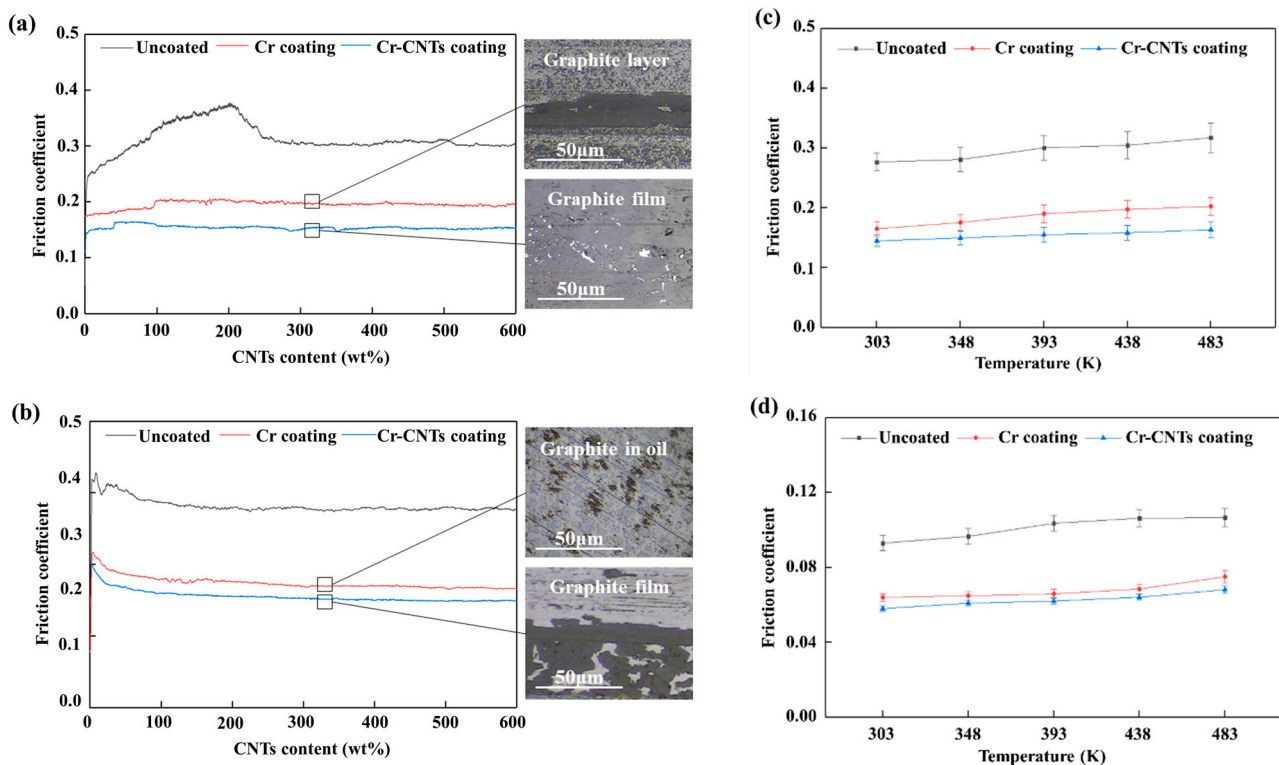


**Figure 9.** Effect of temperature on friction coefficient: (a) grinding process under dry friction condition, (b) grinding process under oil lubrication condition, (c) average friction coefficient under dry friction condition, (d) average friction coefficient under oil lubrication condition.

In the dry friction condition (Figure 9c), the coefficient of friction of the end face of all three materials increases with increasing temperature, and the friction coefficient of the Cr-CNTs coating has the lowest increase with increasing heating temperature. The friction coefficient is about 59.26% lower than that of the uncoated coating and about 14.98% lower than that of the Cr coating at a temperature of 483 K. When the temperature rises, the expansion of the micro-convex body on the end face is enhanced, and the wear increases, so the coefficient of friction increases. The lubrication effect of CNTs between the Cr-CNTs coating end faces is obvious, which reduces the end face wear under high-temperature working conditions. Under oil lubrication conditions (Figure 9d), the value of the friction coefficient of the seal end face coated with Cr-CNTs is more stable with increasing temperature, which is about 43.33% lower than that of the uncoated coating and about 12.46% lower than that of the Cr coating at a temperature of 483 K.

### 3.3. Friction and Wear Mechanism of Cr-CNTs Coatings

Combined with the results of the friction and wear tests and the microscopic morphology observations, the friction and wear mechanism of the end face of the Cr-CNTs coating is shown in Figure 10. The CNTs that are not bound to the Cr particles during laser cladding are distributed in the Cr-CNTs coating in the form of striped particles. Under

dry friction conditions, some of the CNTs near the surface of the coating in the early stage of operation are exposed outside the coating and are prone to fracture and fall off under friction and wear. The striped particles of CNTs generated roll in the wear direction and become a lubricant between the end faces. The CNTs shed from the end face can generate sheet CNTs film under the effect of longer time accumulation and extrusion, which lowers the coefficient of friction and reduces the wear [36]. After a long operation, the graphite ring end face will shed many graphite powders. With the shedding and accumulating graphite powder, a uniform graphite film will be formed between the end faces, which has a stable wear reduction effect. Under oil lubrication conditions, a uniform and stable lubricating oil film between the two end surfaces has an excellent wear-reduction effect. The dislodged graphite powders and CNTs enter the oil film and flow. They are less likely to build up into a film but still have an enhancing effect on the lubrication of the oil film.

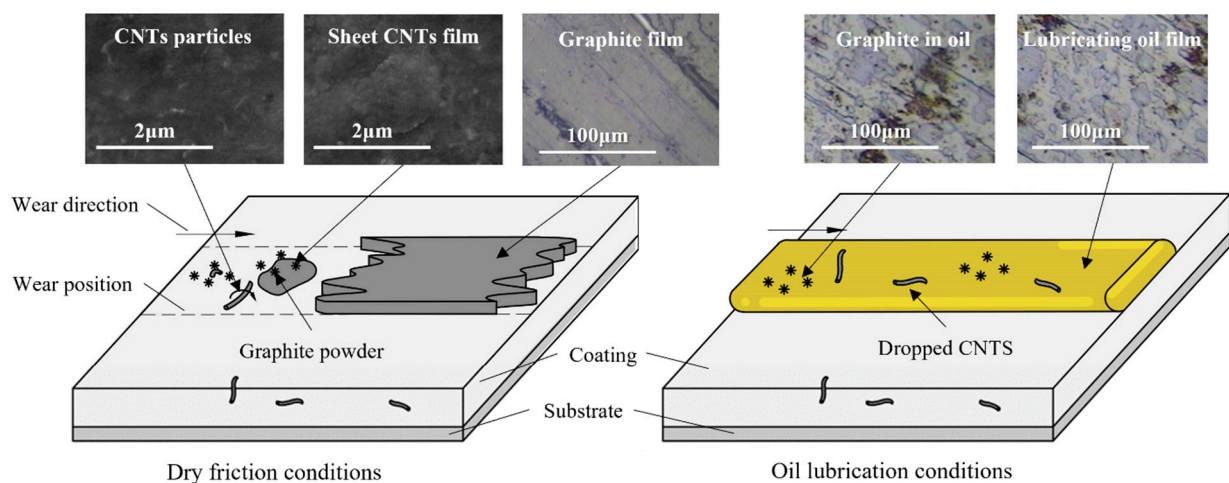


**Figure 10.** Frictional wear mechanism of Cr-CNTs coating.

#### 4. Conclusions

In this study, Cr-CNTs coatings were prepared by laser cladding. The effects of CNTs content and end face material on the tribological performance of the end face were systematically studied, and the friction and wear mechanism of the Cr-CNTs coating was revealed. The theoretical basis for the application of this coating in the field of high-performance mechanical seals was provided, and the following conclusions were obtained:

- (1) The hardness of the coating increases with the content of CNTs. Excessive CNTs will lead to porosity on the end face of the coating and a decrease in the hardness and wear resistance. The Cr-10 wt% CNTs coating has a good grain refinement at the end face and possesses high coating hardness, wear resistance, and self-lubrication. Recommended values for the CNTs content of Cr-CNTs coatings is 10 wt%.
- (2) The coefficient of friction of Cr-CNTs coated seal end faces is low and stable with the temperature under high-temperature conditions. The coefficient of friction of the Cr-CNTs coating is reduced by about 59.26% compared to the uncoated coating and by about 14.98% compared to the Cr coating under dry friction conditions at 483 K. The coefficient of friction of the Cr-CNTs coating is reduced by about 43.33% compared to the uncoated and by about 12.46% compared to the Cr coating under oil lubrication conditions at 483 K.
- (3) The frictional wear mechanism of Cr-CNTs coatings is that the high wear resistance of Cr-CNTs coatings comes from the grain refining effect of CNTs, which improves the comprehensive mechanical properties of the coatings. The self-lubrication comes from the formation of the graphite transfer film and the lubrication effect of CNTs, and the lubrication effect of end-face CNTs comes from the rolled CNTs particles and the sheet CNTs film. The Cr-10 wt% CNTs coating has a good wear reduction effect

under special high-temperature dry friction conditions, which has a high value for engineering applications.

**Author Contributions:** H.Y. proposed a high-performance composite coating and conducted the experimental design and paper writing. S.L. analyzed the experimental results and assisted in preparing the paper. R.M. supervised the friction and wear tests and participated in the revision and touch-up of the thesis. G.Z. carried out the laser melting test and end face micro-morphology observations. A.L. performed the friction wear test and contributed to the data analysis. All authors have read and agreed to the published version of the manuscript.

**Funding:** This research was financially supported by the National Key Research and Development Program of China (Grant No. 2018YFB2000800).

**Institutional Review Board Statement:** Not applicable.

**Informed Consent Statement:** Not applicable.

**Data Availability Statement:** The raw/processed data required to reproduce these findings are available from the corresponding author upon request.

**Conflicts of Interest:** The authors declare that they have no known competing financial interests or personal relationships that could have appeared to influence the work reported in this paper.

## References

1. Lin, Z.; Gao, H.; Zhang, E.; Cao, W.; Li, K. Diamond-Coated Mechanical Seal Remaining Useful Life Prediction Based on Convolution Neural Network. *Int. J. Pattern Recognit. Artif. Intell.* **2020**, *34*, 2051007. [[CrossRef](#)]
2. Luo, Y.; Li, X.; Luo, Z.; Chen, L.; Yang, Y.; Li, J.; Han, G. Enhanced adhesive and anti-corrosive performances of polymer composite coating for rusted metallic substrates by capillary filling. *Prog. Org. Coat.* **2023**, *178*, 107467. [[CrossRef](#)]
3. Guo, D.; Cai, N.; Wu, G.; Xie, F.; Tan, S.; Jiang, N.; Li, H. Improving Pressure–Velocity Limit of Mechanical Seal with Polycrystalline Diamond Coating. *Appl. Sci.* **2020**, *10*, 6090. [[CrossRef](#)]
4. Xie, X.; Hua, X.; Li, J.; Cao, X.; Tian, Z.; Peng, R.; Zhang, P. Synergistic effect of micro-textures and MoS<sub>2</sub> on the tribological properties of PTFE film against GCr15 bearing steel. *J. Mech. Sci. Technol.* **2021**, *35*, 2151–2160. [[CrossRef](#)]
5. Vrček, A.; Hultqvist, T.; Baubet, Y.; Marklund, P.; Larsson, R. Micro-pitting Damage of Bearing Steel Surfaces under Mixed Lubrication Conditions: Effects of Roughness, Hardness and ZDDP Additive. *Tribol. Int.* **2019**, *138*, 239–249. [[CrossRef](#)]
6. Tseluikin, V.N.; Kanaf'eva, O.A. Preparation and Properties of Composite Chromium–Carbon Nanotube Coatings. *Chem. Pet. Eng.* **2015**, *51*, 54–57. [[CrossRef](#)]
7. Zhang, G.Y.; Dang, J.Q.; Zhao, W.G.; Yan, X.T. Tribological behaviors of the thick metal coating for the contact mechanical seal under the water-lubricated conditions. *Ind. Lubr. Tribol.* **2019**, *71*, 173–180. [[CrossRef](#)]
8. Ning, D.; Zhang, A.; Wu, H. Enhanced Wear Performance of Cu-Carbon Nanotubes Composite Coatings Prepared by Jet Electrodeposition. *Materials* **2019**, *12*, 392. [[CrossRef](#)]
9. Li, G.; Liu, Y.; Zhang, Y.; Li, H.; Wang, X.; Zheng, M.; Li, Y. High Temperature Anti-Oxidation Behavior and Mechanical Property of Radio Frequency Magnetron Sputtered Cr Coating. *Metals* **2020**, *10*, 1509. [[CrossRef](#)]
10. Wang, Y.; Chen, Z.; Yu, S.; Pan, N.; Liao, J. Preparation and characterization of dense graphite/glassy carbon composite coating for sealing application. *Mater. Res. Express* **2017**, *4*, 095601. [[CrossRef](#)]
11. Cui, G.; Han, W.; Cui, H.; Liu, Y.; Gao, G.; Kou, Z. Preparation and high-temperature tribological performance of laser clad MoNi coatings with chromium addition. *Surf. Coat. Technol.* **2022**, *440*, 128486. [[CrossRef](#)]
12. Jiahong, L.; Dejun, K. Micro-Structures and High-Temperature Friction-Wear Performances of Laser Cladded Cr–Ni Coatings. *Materials* **2018**, *11*, 137. [[CrossRef](#)] [[PubMed](#)]
13. Wang, D.; Wang, W.Q.; Chen, X.G.; Chi, C.T.; Wang, M.S.; Han, X.; Xie, Y.J. Influence of Cr addition on the interface purification of vacuum brazed NiCr–Cr 3 C 2 coatings on single crystal superalloy. *Surf. Coat. Technol.* **2017**, *325*, 200–209. [[CrossRef](#)]
14. Günen, A.; Bölükbaşı, Ö.S.; Özgürlük, Y.; Özkan, D.; Odabaş, O.; Somunkıran, İ. Effect of Cr Addition on Properties and Tribological Behavior at Elevated Temperature of Boride Layers Grown on Borosintered Powder Metallurgy Alloys. *Met. Mater. Int.* **2023**, *29*, 748–766. [[CrossRef](#)]
15. Guo, P.; Ma, S.; Jiao, M.; Lv, P.; Xing, J.; Xu, L.; Huang, Z. Effect of Chromium on Microstructure and Oxidation Wear Behavior of High-Boron High-Speed Steel at Elevated Temperatures. *Materials* **2022**, *15*, 557. [[CrossRef](#)] [[PubMed](#)]
16. Drozd, M.; Smola, G.; Kyzioł, K.; Migdalska, M.; Jurasz, Z.; Wierzba, B.; Grzesik, Z. Modification of the high-temperature performance of thin chromium coatings deposited on valve steels. *Mater. High Temp.* **2020**, *37*, 145–154. [[CrossRef](#)]
17. Litovka, Y.; Nasraoui, M.; Dolmatov, V. Improved microhardness of chrome galvanic coatings with combining nanodiamonds and nanotubes. *IOP Conf. Ser. Mater. Sci. Eng.* **2019**, *693*, 012012. [[CrossRef](#)]
18. Jia, X.; Wei, F. Advances in Production and Applications of Carbon Nanotubes. *Top. Curr. Chem.* **2017**, *375*, 18. [[CrossRef](#)]

19. Tsai, P.C.; Jeng, Y.R.; Lee, J.T.; Stachiv, I.; Sittner, P. Effects of carbon nanotube reinforcement and grain size refinement mechanical properties and wear behaviors of carbon nanotube/copper composites. *Diam. Relat. Mater.* **2017**, *74*, 197–204. [[CrossRef](#)]
20. Anas, N.S.; Rama Krishna, L.; Dash, R.K.; Vijay, R. Tribological Performance of Al Alloys Dispersed with Carbon Nanotubes or Ni-Coated Carbon Nanotubes Produced by Mechanical Milling and Extrusion. *J. Mater. Eng. Perform.* **2020**, *29*, 1630–1639. [[CrossRef](#)]
21. EL-kashif, E.F.; Esmail, S.A.; Elkady, O.A.; Azzam, B.S.; Khattab, A.A. Influence of carbon nanotubes on the properties of friction composite materials. *J. Compos. Mater.* **2020**, *54*, 2101–2111. [[CrossRef](#)]
22. Reinert, L.; Varenberg, M.; Mücklich, F.; Suárez, S. Dry friction and wear of self-lubricating carbon-nanotube-containing surfaces. *Wear* **2018**, *406–407*, 33–42. [[CrossRef](#)]
23. Lai, C.; Zhong, M.; Xu, W.; Yi, M.; Wu, H.; Huang, M. Influences of B<sub>4</sub>C and carbon nanotubes on friction and wear performance of Cu base self-lubricating composite. *Tribol. Int.* **2023**, *187*, 108726. [[CrossRef](#)]
24. Wang, H.D.; He, P.F.; Ma, G.Z.; Xu, B.S.; Xing, Z.G.; Chen, S.Y.; Wang, Y.W. Tribological behavior of plasma sprayed carbon nanotubes reinforced TiO<sub>2</sub> coatings. *J. Eur. Ceram. Soc.* **2018**, *38*, 3660–3672. [[CrossRef](#)]
25. Wang, G.J.; Cai, Y.P.; Ma, Y.J.; Tang, S.C.; Syed, J.A.; Cao, Z.H.; Meng, X.K. Ultrastrong and Stiff Carbon Nanotube/Aluminum–Copper Nanocomposite via Enhancing Friction between Carbon Nanotubes. *Nano Lett.* **2019**, *19*, 6255–6262. [[CrossRef](#)]
26. Roy, A.; Mu, L.; Shi, Y. Tribological properties of polyimide coating filled with carbon nanotube at elevated temperatures. *Polym. Compos.* **2020**, *41*, 2652–2661. [[CrossRef](#)]
27. Zhou, C.; Li, M.; Chi, J.; Wang, S.; Zhang, M.; Fang, M.; Ren, L. Influence of ball milling process on microstructure and properties of Ni-based coating by laser cladding. *Appl. Phys. A* **2020**, *126*, 955. [[CrossRef](#)]
28. Zhou, K.; Shen, Y. Effects of process parameters and carbon nanotubes content on microstructure and properties of laser cladding composite coatings using Ni-Ti-Cr-carbon nanotubes. *Mater. Res. Express* **2022**, *9*, 096403. [[CrossRef](#)]
29. Han, B.; Chen, Y.; Tan, C.; Jiang, M.; Bi, J.; Feng, J.; Bi, G. Microstructure and wear behavior of laser clad interstitial CoCrFeNi high entropy alloy coating reinforced by carbon nanotubes. *Surf. Coat. Technol.* **2022**, *434*, 128241. [[CrossRef](#)]
30. Yuan, W.; Li, R.; Zhu, Y.; Zhao, Y.; Zhang, X.; Liu, B.; Zhang, B. Structure and properties of nickel-plated CNTs/Fe-based amorphous composite coatings fabricated by high-speed laser cladding. *Surf. Coat. Technol.* **2022**, *438*, 128363. [[CrossRef](#)]
31. Zhou, X.; Chen, Z.; Gu, C.; Wang, J. Thermo-mechanical coupling analysis of the end faces for a mechanical seal under dry friction. *Tribol. Int.* **2021**, *160*, 107050. [[CrossRef](#)]
32. Thakur, L.; Arora, N. An investigation on the development and wear performance of chromium-MWCNTs transformed HVOF sprayed nano-WC-CoCr coatings. *Surf. Coat. Technol.* **2020**, *388*, 125610. [[CrossRef](#)]
33. Liu, J.; Sun, W.; Huang, Y. Effect of carbon nanotubes content on microstructure and properties of WC/Ni laser cladding coatings. *Surf. Eng.* **2021**, *37*, 650–657. [[CrossRef](#)]
34. Parihar, R.S.; Sahu, R.K.; Setti, S.G. Adhesive wear performance of self-lubricating functionally graded cemented tungsten carbide prepared by spark plasma sintering. *Int. J. Refract. Met. Hard Mater.* **2022**, *104*, 105788. [[CrossRef](#)]
35. Zhou, S.; Xu, T.; Hu, C.; Wu, H.; Liu, H.; Ma, X. A comparative study of tungsten carbide and carbon nanotubes reinforced Inconel 625 composite coatings fabricated by laser cladding. *Opt. Laser Technol.* **2021**, *140*, 106967. [[CrossRef](#)]
36. Huang, S.J.; Abbas, A.; Ballóková, B. Effect of CNT on microstructure, dry sliding wear and compressive mechanical properties of AZ61 magnesium alloy. *J. Mater. Res. Technol.* **2019**, *8*, 4273–4286. [[CrossRef](#)]

**Disclaimer/Publisher’s Note:** The statements, opinions and data contained in all publications are solely those of the individual author(s) and contributor(s) and not of MDPI and/or the editor(s). MDPI and/or the editor(s) disclaim responsibility for any injury to people or property resulting from any ideas, methods, instructions or products referred to in the content.